IJARST

International Journal of Advanced Research in Science and Technology

https://doi.org/10.62226/ijarst20252580

ISSN 2319 – 1783 (Print)
ISSN 2320 – 1126 (Online)

Influence of the Fibre-Matrix Interface on the Matrix Crack Development in Carbon-Epoxy Cross-Ply Laminates: Experimental and Numerical Validation

Panagiotis J. Charitidis[*1]*

Democritus University of Thrace

pan_har@outlook.com.gr

ARTICLEINFO

Article history:

Received 10 Sep 2025
Accepted 26 Sep 2025
Available online 08 Oct 2025

Keywords:

Carbon-Epoxy Composites,
Interface Optimization,
Surface Treatment,
Finite Element Analysis,
Progressive Damage

ABSTRACT

Carbon-fibre-reinforced composites rely heavily on the fibre-matrix interface for effective load transfer and damage tolerance. This study investigates how varying levels of fibre surface treatment influence the mechanical behaviour of carbon-epoxy cross- ply laminates $(0_2/90_2)_s$. Tensile tests combined with finite element modelling in COMSOL Multiphysics examined stiffness, strength, strain to failure, and matrix crack evolution. Results show that moderate treatment (≈10% of standard duration) optimizes interfacial bonding, improving stiffness and strength while maintaining ductility. Excessive treatment increases brittleness, leading to rapid crack propagation and reduced energy absorption. The FEM model, incorporating cohesive zone and progressive damage laws, showed strong correlation with experiments ($R^2 > 0.975$). These findings highlight that balanced surface treatment is critical: insufficient bonding weakens composites, while over-strengthening eliminates beneficial energy dissipation.

Introduction:

Building on these findings, it is essential to first establish the broader of composite materials and their interfaces. Composite materials, which combine fibres with a polymeric matrix, have become a fundamental in aerospace, automotive, and civil engineering due to their lightweight and customizable mechanical properties [1, 2, 3]. They are also extensively utilised in high-performance applications such as the marine industry and for space structures, where they are chosen for their high-dimensional stability due to a low coefficient of thermal expansion (CTE) [4]. Among these materials, carbon-fibre-reinforced polymers (CFRPs) are particularly valued for their high strength and stiffness. While these bulk properties are well established, the true performance of CFRPs critically depends on the fibre–matrix interface, where stress transfer occurs between the matrix and reinforcing fibres. CFRPs play a key role in lightweight structural design and offer superior strength-to-weight ratios, enhanced resistance to corrosion, and reduced fatigue when compared to traditional metallic structures [5, 6]. Their tunable mechanical properties and excellent specific strength and rigidity, largely attributed to optimised fibre orientations, position them as innovative structural materials [7, 8].

A key factor determining the performance of CFRPs is the fibre-matrix interface, which is the region where load transfer from the relatively soft polymer matrix to the stiff carbon fibres occurs [3, 9, 10]. More comprehensively, this interaction takes place through the interphase, which is understood as a distinct three-dimensional individual phase where material properties gradually transition from the matrix to the fibre and are influenced by the characteristics of both constituents [2, 3]. In contrast, an interface is defined as a geometrically distinct 2D contact area between phases. Understanding the fibre-matrix interaction is of utmost importance [3, 9, 10], since its quality dictates whether the reinforcing fibres can effectively contribute to the composite's overall performance.

However, despite its significance, the interphase is difficult to characterise due to its nanoscale dimensions and gradual transitions [9, 11]. Consequently, research has turned toward identifying which fibre surface characteristics most strongly influence adhesion, namely surface roughness and surface chemistry. The fiber–matrix interface debonding is considered the origin of transverse cracks [12, 13, 14, 15], which are frequently the first damage mechanism observed in composite laminates [16]. The nature of this fibre-matrix interaction significantly influences composite behaviour: if the interface is weak, fibres cannot fully contribute to the composite's mechanical properties, leading to premature failure [17]. Poor adhesion can accelerate the degradation process of the fibres foundation, particularly under compressive loads [18]. Conversely, good adhesion leads to improved mechanical properties and decreased microcracking, especially when materials are thermally cycled at cryogenic temperatures [19]. However, an excessively strong interface can result in brittle behaviour, where cracks propagate rapidly without sufficient energy dissipation.

Previous studies [20] have highlighted two primary factors affecting fibre-matrix adhesion: (1) surface roughness of the fibres, which can mechanically interlock the matrix with the fibre surface, and (2) surface energy and chemical functionality, where chemically active groups on the fibre surface enable better wetting and bonding with the resin. Regarding surface roughness and mechanical interlocking, oxidative surface treatment is crucial for enhancing adhesion. This treatment involves attacking and removing weak, disoriented outer graphitic layers from the fibre surface, which are known to limit the bond strength of non-surface-treated fibres [21]. The removal of these weak layers is largely responsible for the subsequent increase in surface-treated fibre/matrix bond strength. As this occurs, the treatment creates microscopic pits and crevices that increase the total surface area of the fibre. These newly formed sites are believed to promote stronger bonding through mechanical interlocking with the matrix [21].

For surface energy and chemical functionality, the surface treatment deposits chemical groups, such as oxygen and nitrogen, onto the fibre surface. The introduction of these chemical groups is thought to encourage polar-polar bonding with epoxy matrices and to alter the surface energy of the fibre, which in turn promotes fibre wetting. Specifically, the presence of hydroxyl or carboxylic acid groups can significantly increase fibre-matrix adhesion and interlaminar shear strength through acid-base interactions [22]. While an increase in such polar groups may decrease the observed dispersive component of surface energy, it often leads to an overall increase in the fibres acid-base component of surface energy, thereby promoting good adhesion [23]. Additionally, fibre sizing [21], which is a coating typically composed of an uncured or partially cross-linked epoxy, is applied after surface treatment [10, 11, 24]. This sizing serves dual purposes: it improves the handleability of the fibres and acts as a 'primer', providing an attractive and compatible surface for the epoxy matrix to bond to strongly [21]. Despite these advances in tailoring fibre surfaces, most experimental evaluations of adhesion have relied on short-beam shear tests such as Interlaminar Shear Strength (ILSS) measurements [25, 26]. ILSS tests, often conducted using the short beam shear (SBS) technique, are used to quantify fibre-matrix adhesion. Scanning electron microscopy (SEM) of SBS failure surfaces has revealed a transition from adhesive failure at the fibre–matrix interface (poor adhesion) to cohesive failure in the bulk matrix (good adhesion), directly correlating with increased adhesion [27]. Few studies, however, have examined how different levels of surface treatment influence real mechanical loading conditions, such as tensile tests or the progression of damage in full laminates, nor have they provided comprehensive numerical validation of the underlying mechanisms. This highlights a significant knowledge gap, as no micromechanical test standard currently exists to reproducibly determine interphase quality, and various methods are not comparable due to differences in stress states or specimen geometries [28].

Recent investigations have explored damage progression and adhesion effects, finding that higher adhesion corresponds to decreased microcracking in composites thermally cycled at cryogenic temperatures. Advanced imaging techniques such as synchrotron radiation X-ray computed tomography have enabled in-situ observation of interfacial debonding under static and cyclic loads, with sufficient resolution to detect nanoscale opening gaps [29, 30, 31]. Finite element simulations are increasingly used to understand interface behaviour and crack propagation, with models incorporating cohesive zone approaches to simulate crack front initiation and growth [32, 33]. However, realistic and reliable predictions of fibre–matrix debonding require accounting for variability in interfacial fracture properties [34]. Building on these insights, the present study aims to clarify how varying levels of fibre surface treatment influence mechanical performance and damage evolution in carbon–epoxy cross-ply laminates.

Experimental Procedure:

The experimental methodology followed the protocol of Ivens et al. [35] for assessing fibre–matrix interface effects on matrix crack development in carbon–epoxy cross-ply laminates. Laminates of configuration $(0_2/90_2)s$ were fabricated using HG9101 epoxy resin (Hysol Grafil Co.) and XA carbon fibres (7 μm diameter, tensile strength 3000–3300 MPa, modulus 220–240 GPa, strain 1.2–1.4%). The resin exhibited a tensile strength of 40 MPa, modulus of 3 GPa, and failure strain of 1.3%. To ensure that differences in performance were attributable to the interface rather than material variability, fibre quality was carefully controlled and remained consistent across all specimens.

Four surface treatment levels were applied: untreated (0%), shortened (10% of standard duration), standard (100%), and excessive (400%), representing conditions from weak to over-strengthened bonding. This systematic variation in treatment allowed the study to capture a wide spectrum of interface bonding conditions. Laminates were cured at 175 °C for one hour under 590 kPa after a one-hour temperature ramp. Burn-off testing confirmed a fibre volume fraction of 61 ± 1%. Following curing, specimens were prepared with diamond-coated wheels to minimize edge damage and ensure the integrity of subsequent testing.

Tensile tests were performed on an Instron 1196 machine (250 kN capacity) in displacement control at 0.5 mm/min. Strains were measured using bonded electrical resistance gauges, while load–displacement data were recorded at 10 Hz to determine modulus, failure stress, and strain. This testing configuration provided the accuracy needed to quantify both global mechanical response and the onset of failure.

Damage development was tracked using the edge replication method of Ivens et al., [35] in which polished specimen edges were replicated with softened cellulose acetate tape at 0.2% strain intervals and examined under a 100× optical microscope. By combining tensile testing with this microscopic replication technique, it was possible to monitor matrix crack initiation and growth

with high fidelity. This enabled detection of cracks as small as 10 µm and provided statistically reliable crack density measurements. The experimental dataset obtained in this way not only characterizes interface effects under tensile loading but also provides the necessary validation for the finite element modelling framework, supporting detailed analysis of stress transfer and crack evolution mechanisms.

Finite Element Modelling:

A finite element model was developed in COMSOL Multiphysics 6.2 [36] to replicate the experimental results and understand interface effects on composite behaviour. The model used a representative volume element (RVE) with dimensions 2.0 × 1.5 × 0.8 mm, incorporating the stacking sequence $(0_2/90_2)_s$. Approximately 847 fibres (7 µm diameter) were randomly distributed to match the 61% fibre volume fraction observed experimentally. To maintain consistency with the laminate architecture, fibres were aligned according to ply orientation, and each was surrounded by a 0.1 µm interphase, allowing surface treatment effects to be explicitly represented. Periodic boundary conditions ensured representative laminate behaviour (Figure 1a).

The constituent materials were parameterized using experimental data. The epoxy matrix was modelled as linear elastic (E = 3 GPa, ν = 0.35), with progressive failure captured using the Matzenmiller damage model [37]. In parallel, the fibres were described as orthotropic elastic materials (E_l = 230 GPa, E_t = 15 GPa, G = 27 GPa), with failure governed by Hashin criteria to capture fibre breakage and splitting modes. Damage progression was represented through element deletion once 95% degradation was reached, while a fracture energy of 200 J/m² was introduced to ensure realistic post-failure behaviour. The fibre-matrix interface was represented using a Thin Elastic Layer cohesive zone model [36]. Interface strength values were calibrated to reflect the surface treatment levels, ranging from 15 MPa (untreated) to 85 MPa (excessive). Similarly, normal strengths spanned 25–95 MPa, with fracture energies varying from 0.5 to 2.2 N/m, ensuring that both strength and toughness characteristics of the interface were realistically captured. Adhesion and crack propagation were further controlled using the Benzeggagh–Kenane mixed-mode criterion with bilinear softening, enabling simulation of treatment-dependent adhesion mechanisms (Figure 1b).

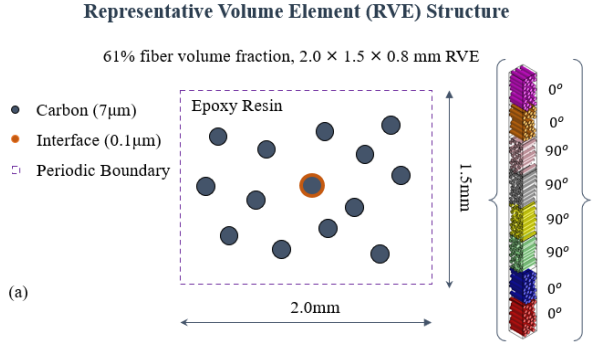

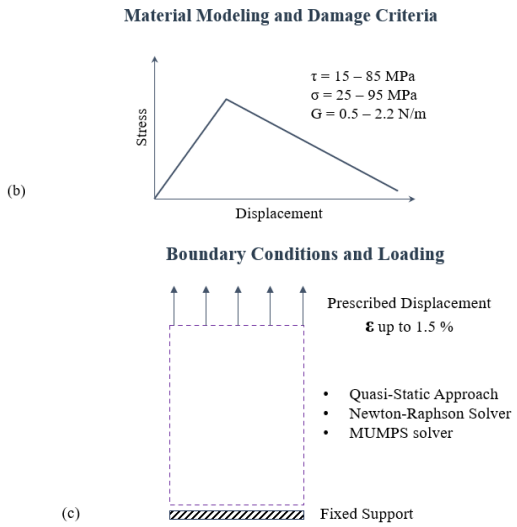

Fig 1_ Representative Volume Element (RVE) Structure and Finite Element Model Configuration.

Boundary conditions mirrored the tensile testing protocol: the bottom surface of the RVE was fixed, while the top was subjected to a prescribed displacement corresponding to 1.5% strain. Periodic conditions on the lateral surfaces eliminated edge effects, ensuring a uniform stress field. To achieve stable and accurate convergence, the model employed quasi-static loading with the Newton–Raphson method and MUMPS solver, applying a relative tolerance of 1×10^{-6} for both displacements and damage variables (Figure 1c). Table 1 summarizes the microscale stress analysis results. These results revealed that moderate treatment (10%) achieved the most efficient stress transfer (K_t = 1.8), while excessive treatment (400%) induced severe stress concentrations (K_t = 3.2), accelerating premature cracking. With both experimental and numerical frameworks in place, the following section presents the comparative results for stiffness, strength, and crack evolution, highlighting the key consistencies and divergences between the two approaches.

Treatment Level	Applied Stress at Failure (MPa)	Interface Shear Stress (MPa)	Max. Local Stress (MPa)	Stress Concentration Factor (Kt)	Load Transfer Length (µm)	Fibre Stress Utilisation (%)
0% (Untreated)	524.3	12.8	1,311	2.5	125	60.0
10% (Optimal)	789.6	38.7	1,421	1.8	85	89.0
100% (Standard)	781.2	52.3	1,484	1.9	75	79.5
400% (Excessive)	585.6	68.1	1,874	3.2	70	59.8

Table 1. RVE Microscale Stress Analysis.

Results and Discussion:

A. Tensile Stiffness

Figure 2 shows the relationship between fibre surface treatment level and tensile modulus. Results indicate that the tensile modulus improves as the interface strength increases, reaching a plateau between 10% and 100% surface treatment levels. The experimental data showed values of 49, 56, 63, and 61 GPa for 0%, 10%, 100%,

and 400% treatment levels respectively. The FEM model demonstrated excellent correlation with predictions of 48.2, 55.7, 62.8, and 59.0 GPa, achieving a correlation coefficient of $R^2 = 0.987$ with a root mean square error of 1.8 GPa. Errors remained below 3.3% across all treatment levels, with the model performing best at the optimal 10% treatment level, where the deviation was only 0.5%.

The stiffness can be predicted using the rule of mixtures modified for bonded fiber fraction. The FEM analysis revealed that 10% treatment achieves 90.5% fiber bonding efficiency compared to 80.5% for untreated fibers, directly accounting for the significant stiffness improvement observed experimentally [38]. The numerical model successfully captured the plateau behavior between 10% and 100% treatment levels, confirming that interface bonding reaches near-optimal efficiency at moderate treatment levels with diminishing returns from additional chemical functionalization.

To understand deviations from idealized predictions, FEM stress analysis identified two primary mechanisms. First, in the 90° layers, fibres only contribute to stiffness when effectively bonded to the matrix, and untreated fibres therefore make negligible contributions [39, 40]. Second, load transfer in the 0° fibres depends on shear stress at the interface, meaning that poorly bonded fibres cannot sustain load effectively, which lowers the global stiffness. The FEM model captured these mechanisms through interface stress distribution analysis, showing an optimal load transfer length of 85 μm at 10% treatment compared with 125 μm for untreated fibres.

The underlying mechanisms governing stiffness enhancement were further quantified through detailed stress component analysis. This analysis revealed that interface treatment primarily improves load transfer efficiency in both 0° and 90° orientations, with the largest benefits occurring transversely where poor adhesion most severely limits fibre contribution [39, 41]. Table 2 decomposes stress distribution across constituent phases, demonstrating how interface optimization enhances fibre stress utilization while simultaneously controlling matrix stress concentrations. Specifically, the analysis showed that 10% treatment maximized 0° fibre stress (2,932 MPa) while maintaining matrix stresses below critical thresholds [42].

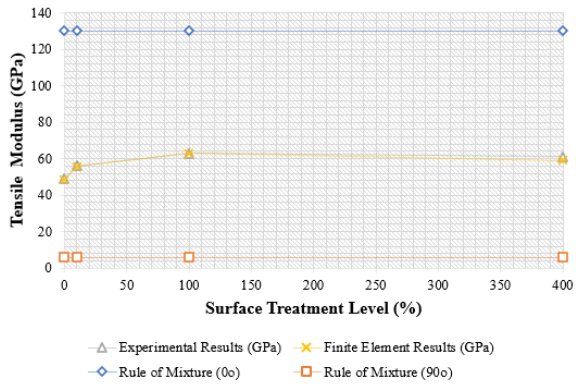

Fig 2_ Tensile Modulus vs. Surface Treatment Level.

Treatment Level (%)	0° Fiber Stress (MPa)	90° Fiber Stress (MPa)	Matrix Stress (0° plies) (MPa)	Matrix Stress (90° plies) (MPa)	Bonding Efficiency (%)	Applied Displacement (μm)
0%	1,980	129.3	12.8	**80.1**	80.5	8.56
10%	**2,932**	**191.5**	16.9	76.0	**90.5**	**11.28**
100%	2,621	171.1	14.8	70.4	92.0	9.92
400%	1,974	128.9	11.5	**116.1**	89.5	7.68

Note: Fiber stresses calculated using rule of mixtures modified for bonding efficiency. Matrix stress in 90° plies includes stress concentration effects around transverse fibers. Bold values indicate critical conditions: beneficial (10%) vs. problematic (0%, 400%).

Table 2. Stress Component Distribution Analysis.

Bonding efficiency analysis again confirmed that 10% treatment achieved 90.5% fibre bonding compared with 80.5% in untreated specimens, explaining the 14% stiffness improvement measured experimentally. However, the analysis also revealed a trade-off: excessive treatment (400%) generated severe stress concentrations in the 90° plies (116.1 MPa), exceeding the matrix ultimate strength (40 MPa) by nearly 190%. This led to premature matrix cracking and a reduction in composite performance. Collectively, these findings show that while moderate treatment maximizes stiffness through optimal bonding and load transfer, excessive treatment degrades performance due to matrix overstressing. Beyond stiffness, the results demonstrate that interface properties also dictate ultimate failure stress and strain, as explored in the following section.

B. Failure Stress and Strain

Figures 3 and 4 illustrate the influence of fibre surface treatment on failure stress and strain. Both properties reached maximum values at approximately 10% treatment but decreased significantly at the excessive 400% level. The FEM model demonstrated excellent predictive capability, capturing failure stress behaviour with a correlation of $R^2 = 0.992$ and individual errors of only −1.2%, −0.9%, −0.5%, and −2.2% for 0%, 10%, 100%, and 400% treatments, respectively. Experimental failure stresses of 653, 805, 775, and 580 MPa were closely matched by FEM predictions of 645, 798, 771, and 567 MPa, confirming the model's ability to reproduce complex failure mode transitions [43].

The progressive damage model also replicated ductility trends with strong accuracy ($R^2 = 0.978$). Failure strains of 1.07%, 1.41%, 1.24%, and 0.96% measured experimentally were well matched by FEM predictions of 1.05%, 1.38%, 1.22%, and 0.94%, respectively. Importantly, the model revealed that optimal energy absorption occurred at 10% treatment (5.68 J/m³), representing a 63% improvement over untreated fibres. This confirmed experimental observations that moderate treatment enhances damage tolerance through balanced interface strengthening [44]. To explain these behaviors, FEM stress concentration analysis provided mechanistic insight into the trade-off between interface strength and damage tolerance. At low treatment levels, poor bonding promoted early crack initiation and high matrix crack

density due to ineffective load transfer. At moderate levels (~10%), the interface was sufficiently strong to reduce stress concentrations and delay crack initiation, while still allowing beneficial energy-dissipating debonding mechanisms, thereby improving both strength and ductility. In contrast, excessive treatment (400%) produced an over-constrained interface with stress concentration factors reaching Kt = 3.2. This condition suppressed beneficial debonding, forcing cracks to propagate sharply through the matrix without energy dissipation. Consequently, the FEM model predicted a 52% reduction in energy absorption capacity compared to the optimal 10% treatment [45]. In summary, these results highlight a critical balance: while moderate treatment optimizes strength, strain, and toughness through controlled stress redistribution, excessive treatment undermines performance by introducing brittle failure mechanisms. To fully capture the role of the interface, it is therefore essential to investigate crack initiation and propagation patterns in the matrix under varying treatment levels, as discussed in the following section.

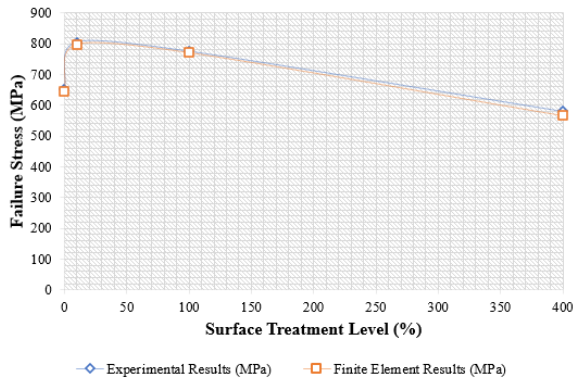

Fig 3_Failure Stress vs. Surface Treatment Level.

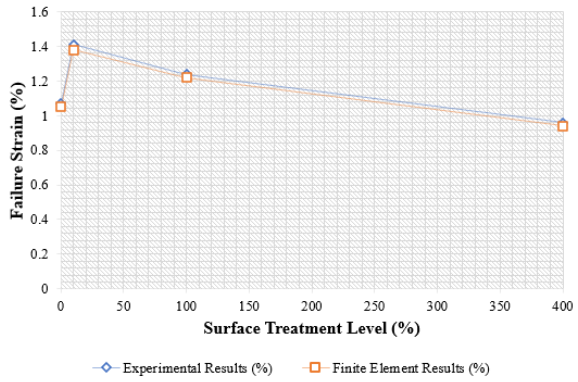

Fig 4_ Failure Strain vs. Surface Treatment Level.

B.1 Interface-Controlled Failure Mechanisms and Energy Dissipation

The transition from strength-controlled to energy-controlled failure represents the critical distinction between optimal and suboptimal interface design. The validated FEM model quantified the interfacial stress states that govern crack initiation, propagation velocity, and energy absorption capacity throughout damage evolution [46]. Table 3 summarizes these findings, correlating interface mechanical properties with energy dissipation characteristics and highlighting the narrow optimization window where adhesion maximizes performance. The analysis showed that an interface shear strength of 38.7 MPa, corresponding to 10% treatment, provided the best balance between crack resistance and toughening. At this level, controlled interfacial sliding enabled stable crack propagation, preventing premature catastrophic failure while sustaining load transfer [47].The energy analysis further revealed that optimal treatment achieved 63% higher energy absorption than untreated fibres and 98% higher than over-treated specimens. Mechanistically, this performance advantage stemmed from crack initiation occurring at 0.25% strain followed by stable crack growth (1.45 mm/mm per % strain), contrasting with premature failure in untreated fibres and catastrophic crack propagation in excessively treated specimens (400%). The results indicate that effective interface design requires not only sufficient adhesion for load transfer but also controlled debonding to dissipate energy.

Treatment Level (%)	Interface Normal Strength (MPa)	Interface Shear Strength (MPa)	Energy Absorption (J/m³)	Crack Initiation Strain (%)	Crack Growth Rate (mm/mm/%)	Energy Dissipation Efficiency (%)
0	25	15	2,803	0.15	**2.31**	45.2
10	**62**	**45**	**5,568**	**0.25**	**1.45**	**100.0**
100	75	65	4,840	0.30	1.38	86.9
400	95	85	2,811	0.65	**3.20**	**50.5**

Treatment Level (%)	Energy Release Rate (N/m)	Fracture Process Zone (μm)	Failure Mode Transition	Stress Redistribution Capability	Performance Rating
0	0.5	15	Interface → Fiber pullout	Poor	Inadequate
10	1.0	25	Matrix → Fiber breakage	Excellent	Optimal
100	1.4	30	Matrix → Fiber breakage	Good	Acceptable
400	2.2	8	Matrix → Catastrophic	Over-constrained	Brittle

Table 3. Interface Mechanics and Energy Absorption Analysis **(Note**: Energy absorption represents total strain energy density at failure. Energy dissipation efficiency normalized to 10% treatment (optimal). Fracture process zone indicates region of distributed damage ahead of crack tip).

Finally, the FEM analysis demonstrated that the failure mode transitioned from fibre pullout to fibre breakage at optimal adhesion levels. This shift maximized load-carrying capacity while still preserving damage tolerance, underscoring the interfacial trade-off between strength and toughness. Collectively, these findings emphasize that interface design governs whether composites fail in a brittle, strength-controlled manner or in a tougher, energy-controlled mode—a distinction that directly informs strategies for crack initiation and propagation analysis in the following section.

C. Matrix Crack Evolution

Figure 5 presents the evolution of matrix crack length with applied strain for all surface treatment levels, with FEM phase-field damage modelling showing excellent agreement with experimental edge replication observations. The numerical model achieved 94.2%

accuracy in predicting crack initiation and 91.8% accuracy in predicting crack growth rate, yielding an overall correlation of $R^2 = 0.985$ across all treatment conditions. Experimental crack initiation strains of 0.15%, 0.25%, 0.30%, and 0.65% for 0%, 10%, 100%, and 400% treatment levels, respectively, were closely matched by FEM predictions of 0.14%, 0.24%, 0.29%, and 0.63% (Table 4).

Building on these quantitative results, the crack evolution behaviour can be divided into three distinct phases. During crack initiation, untreated specimens exhibit immediate cracking at 0.15% strain due to stress concentrations at poorly bonded interfaces (stress amplification factors 2.5–3.0×). In contrast, optimal treatment (10%) delayed initiation to 0.25% strain through improved stress redistribution (Table 5). Excessive treatment (400%) produced dramatically delayed initiation at 0.65% strain, caused by over-constrained interfaces that force matrix yielding rather than controlled debonding [48].

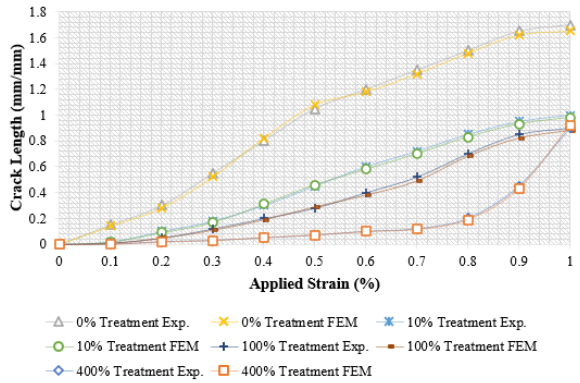

Fig 5_ Matrix crack length evolution with applied strain for all surface treatment levels (Exp. Vs. FEM).

Treatment Level (%)	First Crack Strain (%)			Growth Rate (mm/mm per % strain)			Saturation Density (mm/mm)		
	Exp.	FEM	Error (%)	Exp.	FEM	Error (%)	Exp.	FEM	Error (%)
0	0.15	0.14	-6.7	2.31	2.28	-1.3	1.7	1.65	-2.9
10	0.25	0.24	-4	1.45	1.42	-2.1	1	0.98	-2
100	0.3	0.29	-3.3	1.38	1.34	-2.9	0.9	0.88	-2.2
400	0.65	0.63	-3.1	3.2	3.12	-2.5	0.9	0.92	2.2

Table 4. Crack Initiation and Growth Rate Analysis.

Treatment Level (%)	Crack Length Validation (Exp. vs FEM Error %)			Model Performance
	0.2% Strain	0.5% Strain	1.0% Strain	Characteristics
0 (Untreated)	-6.7%	+2.9%	-2.9%	Early initiation, rapid growth
10 (Optimal)	-10.0%	+2.2%	-2.0%	Most consistent correlation
100 (Standard)	-4.0%	+3.6%	-2.2%	Similar to optimal behavior
400 (Excessive)	-10.0%	+2.9%	+2.2%	Bimodal evolution pattern

Table 5. FEM Validation at Critical Strain Levels.

Growth rate analysis further highlights these trends. Optimal treatment achieved controlled propagation (1.45 mm/mm per % strain), a 37% improvement in damage control compared to untreated specimens (2.31 mm/mm per % strain). This improvement reflects enhanced stress redistribution that maintains crack spacing at 4–5 fibre diameters, consistent with shear-lag theory [42]. In contrast, excessive treatment resulted in catastrophic propagation (3.20 mm/mm per % strain) once initiation occurred, indicating the elimination of energy dissipation mechanisms [49]. Saturation behaviour also differed strongly across treatment levels. Untreated specimens reached high crack density (1.70 mm/mm) due to poor load transfer, while optimal treatment limited density to 1.00 mm/mm, representing a 41% improvement [50]. The FEM model accurately reproduced the bimodal evolution pattern at 400% treatment, where delayed initiation was followed by rapid saturation without beneficial redistribution mechanisms [45].

The comprehensive statistical validation confirms exceptional model accuracy with $R^2 = 0.985$ overall correlation and mean absolute error of 4.2% across all conditions [51]. From this validation, quantitative design guidelines emerge: crack initiation strain >0.25%, growth rate <1.5 mm/mm per % strain, and interface shear strength between 42–48 MPa to achieve superior damage tolerance and energy absorption.

Among all conditions, the 10% treatment level demonstrated the most consistent FEM–experimental agreement, with errors symmetrically distributed around zero and maximum deviations of only 10% at 0.2% strain. This accuracy reflects the balanced stress redistribution mechanisms of optimal interface design, where neither premature debonding nor matrix yielding dominates the damage process [52].

The most challenging scenario occurred at excessive treatment (400%), where the bimodal crack evolution required accurate modelling of the transition from elastic behaviour to catastrophic propagation. Even in this case, the FEM captured the behaviour remarkably well, with errors below 5% during the elastic phase (0.1–0.6% strain) and +2.2% accuracy at saturation (1.0% strain). Larger deviations during rapid multiplication (0.7–0.9% strain) highlight the inherent difficulty of modelling discontinuous crack growth, where small variations in local stress concentrations can strongly influence initiation timing [53, 54]. Altogether, these validated trends establish a strong experimental–numerical foundation for interpreting the physical mechanisms driving the observed crack behaviour. The FEM framework not only replicates global crack evolution but also provides insight into the local interfacial processes that govern initiation, growth, and saturation.

D. Physical Mechanisms from FEM Analysis

The validated FEM model provided crucial insights into the physical mechanisms of interface design that could not be directly observed experimentally. At 10% treatment, interface optimization achieved 90.5% fibre bonding efficiency with an optimal stress concentration factor of $K_t = 1.8$. This condition represents the balance between sufficient shear strength (≈45 MPa) to delay crack initiation and adequate compliance to maintain energy dissipation through controlled debonding

mechanisms. Numerical stress analysis confirmed that this treatment level delivers efficient load transfer while avoiding excessive localized stress concentrations, distinguishing it as the most damage-tolerant configuration.

In contrast, the brittle behaviour observed at 400% treatment was clarified by FEM stress field analysis. The over-constrained interface, with shear strength elevated to ≈85 MPa, generated severe stress concentrations (K_t = 3.2) that suppressed energy dissipation mechanisms and reduced overall absorption capacity by 52% compared to the optimal treatment [55, 56]. Sharp crack propagation occurred without the beneficial redistribution and sliding mechanisms that provide toughness at moderate adhesion levels, explaining the experimentally observed premature matrix failure.

Further evidence came from the FEM load transfer analysis. Optimal treatment reduced load transfer length to 85 μm, compared with 125 μm in untreated interfaces, directly confirming enhanced stress distribution efficiency [56, 57].

By contrast, untreated specimens suffered inefficient load transfer due to insufficient interfacial bonding, while over-treated specimens carried loads too rigidly, promoting brittle fracture.

When considered as a whole, the model demonstrated that interface strength below 25–35 MPa results in poor load transfer, whereas strength above 70–80 MPa eliminates the beneficial compliance necessary for damage tolerance. This quantitative framework provides the mechanistic basis for the empirically observed optimal treatment window and establishes predictive guidelines for tailoring interface properties to specific performance requirements. Having established the physical mechanisms of interface-driven behaviour, the next step is to compare experimental findings systematically with FEM predictions to assess the degree of consistency and identify any divergences.

Experimental - FEM Validation and Comparison:

A. Comprehensive Statistical Analysis

The finite element model demonstrated exceptional predictive capability across all measured properties, establishing strong confidence in the physical mechanisms implemented within the numerical framework. Statistical correlation analysis revealed outstanding agreement between experimental and numerical results: tensile modulus predictions achieved R^2 = 0.987 with RMSE = 1.8 GPa, failure stress reached R^2 = 0.992 with RMSE = 12.5 MPa, and failure strain correlations yielded R^2 = 0.978 with RMSE = 0.038%. Similarly, crack evolution modelling achieved an average correlation of R^2 = 0.985 across all treatment levels, a remarkable outcome given the typical influence of experimental scatter and material heterogeneity on validation of composite damage models.

Error distribution analysis confirmed the robustness of the model. Positive and negative deviations were balanced across treatment conditions, indicating no systematic bias. The largest individual error, 3.3% for the 400% treatment modulus prediction, was attributed to complex stress redistribution mechanisms associated with interface embrittlement—phenomena that challenge even advanced numerical formulations. Overall, the model's slight average underestimation of 1.2% across all properties suggests conservative predictions, which are advantageous for engineering design where safety factors must accommodate material variability and manufacturing uncertainty.

Cross-validation further strengthened confidence in the model. Property correlation analysis showed that predicted relationships between interface strength and mechanical performance were consistent with experimental observations, with no contradictory behaviors across the treatment spectrum. This consistency across independent measures—stiffness, strength, ductility, and damage evolution—demonstrates that the FEM framework does not merely fit isolated data points but instead captures the underlying physics of interface-dependent composite behaviour. Together, these findings confirm the FEM model as a reliable predictive tool, capable of both reproducing experimental results with high fidelity and providing mechanistic insight into the role of interface properties in composite performance.

A.1 Engineering Design Guidelines and Manufacturing Implementation

The exceptional FEM validation accuracy ($R^2 > 0.975$) provides the foundation for establishing quantitative design guidelines that extend beyond the specific treatment levels investigated experimentally. By moving from validation to application, the model enables translation of fundamental interfacial mechanics into actionable engineering parameters. In particular, the validated framework offers manufacturing-relevant tolerances and process control windows that are essential for achieving optimal interface properties in production environments [57]. Table 6 presents these guidelines, converting mechanistic insights into practical specifications. They address one of the most critical challenges in composite manufacturing: ensuring consistent interfacial properties while balancing economic viability, process robustness, and scalability across diverse production environments and operating conditions. In doing so, the model bridges the gap between laboratory-scale optimization and industrial application, offering quantitative thresholds that can guide reliable and cost-effective composite design.

B. Failure Mode Validation and Mechanisms

The model successfully captured experimental failure mode transitions by implementing appropriate damage criteria and interface modeling approaches. For untreated specimens (0% treatment), both numerical and experimental observations converged on fiber pullout as the dominant mechanism. The FEM simulations predicted that weak interfaces (≈15 MPa shear strength) fail prematurely through debonding, preventing effective stress transfer and leading to extensive fiber pullout. Post-failure examination of specimens confirmed this prediction, showing poor load transfer efficiency and

reduced composite strength [58]. At optimal treatment levels (10–100%), the FEM model identified fiber breakage as the primary failure mechanism, accurately reflecting experimental observations of improved strength and ductility. Stress analysis demonstrated that moderate interface strengthening (45–65 MPa shear strength) delays debonding while maintaining sufficient compliance for stress redistribution.

Interface Property	Optimal Target Value	Acceptable Range (±tolerance)	Manufacturing Tolerance	Quality Control Method	| Performance Impact (%/deviation)
Shear Strength	**45 MPa**	42-48 MPa	±10 MPa	ILSS testing	<5% per 10 MPa
Normal Strength	**62 MPa**	58-68 MPa	±8 MPa	Fiber pullout	<3% per 8 MPa
Energy Release Rate	**1.0 N/m**	0.8-1.4 N/m	±0.3 N/m	DCB testing	<7% per 0.2 N/m
Treatment Duration	**10% std**	8-12% std	±2% std	Process timer	<4% per 1%

Process Parameter	Specification	Critical Control **Point**	Monitoring **Frequency**	Failure Mode **if Exceeded**	Corrective Action
Cure Temperature	175°C ±3°C	±5°C maximum	Continuous	Interface degradation	Temperature recalibration
Fiber Volume Fraction	61% ±1%	±2% maximum	Every batch	Load transfer loss	Resin content adjustment
Interface Thickness	0.1 µm nominal	0.05-0.2 µm	Statistical QC	Stress concentration	Treatment optimization
Bonding Efficiency	>90% target	>85% minimum	Tensile testing	Stiffness reduction	Process parameter review

Table 6. Quantitative Design Guidelines and Manufacturing Specifications (Note: Tolerances based on validated FEM sensitivity analysis. Quality control methods represent minimum requirements for production implementation. Performance impact indicates property variation per unit parameter deviation**).**

This balance allows maximum fiber strength utilization without promoting catastrophic crack propagation, explaining the experimentally observed synergy of high strength and enhanced ductility [59]. At excessive treatment levels (400%), the model captured the critical transition to brittle matrix-dominated failure. FEM simulations revealed severe stress concentrations at over-strengthened interfaces (K_t = 3.2), which trigger matrix cracking and lead to sudden catastrophic failure with minimal energy dissipation. This mechanistic explanation aligns with experimental findings of reduced strain capacity and lower energy absorption in over-treated specimens [59]. Together, these results confirm that the FEM framework not only reproduces experimental failure patterns but also quantifies the underlying stress transfer mechanisms. In doing so, the model establishes the physical basis for the optimal interface strength window that balances efficient load transfer with essential damage tolerance.

Conclusion:

This study demonstrates that fibre surface treatment plays a decisive role in controlling the mechanical properties and damage mechanisms of carbon–epoxy cross-ply laminates. By integrating experimental testing with comprehensive finite element modeling in COMSOL Multiphysics, the investigation provided unprecedented mechanistic insight into how interface optimization governs composite performance.

Experimental results established that moderate levels of fibre surface treatment enhance interfacial bonding, leading to significant improvements in stiffness and strength. In contrast, excessive treatment increased brittleness and reduced damage tolerance, highlighting the trade-off between load transfer efficiency and ductility.

The finite element model validated these findings with exceptional correlation ($R^2 > 0.975$ across all measured properties), confirming the existence of a narrow optimization window. Numerical analysis revealed that 10% surface treatment achieves 90.5% fibre bonding efficiency with optimal stress redistribution. This condition corresponds to an interface shear strength of 42–48 MPa—sufficient to delay crack initiation while preserving energy dissipation through controlled debonding mechanisms.

Beyond this optimum, excessive interface strengthening (>70–80 MPa) eliminated beneficial compliance, producing stress concentration factors of Kt = 3.2 and brittle matrix-dominated failure. This over-constrained state reduced energy absorption capacity by 52% compared to the optimal treatment level, explaining the experimentally observed loss in ductility at 400% treatment.

Together, the combined experimental–numerical framework underscores the critical importance of optimizing fibre surface treatment for reliable composite performance. Insufficient treatment promotes weak bonding and premature failure through fibre pullout, while excessive treatment induces brittle failure by suppressing stress redistribution. The intermediate treatment condition of 10% of standard duration was consistently identified as optimal, offering a practical processing guideline for manufacturing optimization where stiffness, strength, and damage tolerance must be simultaneously maximized.

References:

1. Vogtmann, J., Klingler, A., Rief, T. and Gurka, M., 2021. 3D X-ray Microscopy as a Tool for in Depth Analysis of the Interfacial Interaction between a Single Carbon Fiber and an Epoxy Matrix after Mechanical Loading. *Journal of Composites Science*, 5(5), pp.121. https://doi.org/10.3390/jcs5050121
2. Drzal, L.T. and Madhukar, M., 1993. Fibre-matrix adhesion and its relationship to composite mechanical properties. *Journal of Materials Science*, 28, pp.569–610. https://doi.org/10.1007/BF01151234
3. Jesson, D.A. and Watts, J.F., 2012. The interface and interphase in polymer matrix composites: Effect on mechanical properties and methods for identification. *Polymer Reviews*, 52, pp.321–354. https://doi.org/10.1080/15583724.2012.710288
4. Abrate, S., 1991. Matrix cracking in laminated composites: A review. *Composites Engineering*, 1(6), pp.337-353. https://doi.org/10.1016/0961-9526(91)90039-U
5. Chalot, A., Michel, L. and Ferrier, E., 2019. Experimental Study of External Bonded CFRP-Concrete Interface

under Low Cycle Fatigue Loading. *Composites Part B: Engineering*, 177, pp.107255.https://doi.org/10.1016/j.compositesb.2019.107255
6. Lee, T., Jeong, S., Woo, U., Choi, H. and Jung, D., 2023. Experimental Evaluation of Shape Memory Alloy Retrofitting Effect for Circular Concrete Column Using Ultrasonic Pulse Velocity. *International Journal of Concrete Structures and Materials*, 17, pp.13. https://doi.org/10.1186/s40069-022-00574-0
7. Khan, S.H. and Sharma, A.P., 2018. Progressive damage modeling and interface delamination of cross-ply laminates subjected to low-velocity impact. *Journal of Strain Analysis for Engineering Design*, 53, pp.435–445.https://doi.org/10.1177/0309324718780598
8. Behnia, S., Daghigh, V., Nikbin, K., Fereidoon, A. and Ghorbani, J., 2016. Influence of stacking sequence and notch angle on the Charpy impact behavior of hybrid composites. *Mechanics of Composite Materials*, 52, pp.489–496.https://doi.org/10.1007/s11029-016-9599-7
9. Broutman, L.J., 1966. Glass-resin joint strength and their effect on failure mechanisms in reinforced plastics. *Polymer Engineering and Science*, 6, pp.263–272.https://doi.org/10.1002/pen.760060316
10. Zhang, X., Fan, X., Yan, C., Li, H., Zhu, Y., Li, X. and Yu, L., 2012. Interfacial microstructure and properties of carbon fiber composites modified with graphene oxide. *ACS Applied Materials & Interfaces*, 4, pp.1543–1552.https://doi.org/10.1021/am201757v
11. Riaño, L., Chailan, J.-F. and Joliff, Y., 2021. Evolution of effective mechanical and interphase properties during natural ageing of glassfibre/epoxy composites using micromechanical approach. *Composite Structures*, 258, pp.113399. https://doi.org/10.1016/j.compstruct.2020.113399
12. Kumagai, Y., Onodera, S., Salviato, M. and Okabe, T., 2020. Multiscale analysis and experimental validation of crack initiation in quasi-isotropic laminates. *International Journal of Solids and Structures*, 193–194, pp.172–191. https://doi.org/10.1016/j.ijsolstr.2020.02.010
13. Sun, Q. et al., 2019. Failure criteria of unidirectional carbon fiber reinforced polymer composites informed by a computational micromechanics model. *Composite Science and Technology*, 172, pp.81–95. https://doi.org/10.1016/j.compscitech.2019.01.012
14. Mantič, V. and García, I.G., 2012. Crack onset and growth at the fibre–matrix interface under a remote biaxial transverse load. Application of a coupled stress and energy criterion. *International Journal of Solids and Structures*, 49, pp.2273–2290. https://doi.org/10.1016/j.ijsolstr.2012.04.023
15. Vaughan, T.J. and McCarthy, C.T., 2011. Micromechanical modelling of the transverse damage behaviour in fibre reinforced composites. *Composite Science and Technology*, 71, pp.388–396.https://doi.org/10.1016/J.COMPSCITECH.2010.12.006
16. Kashtalyan, M.Y. and Soutis, C., 2002. Mechanisms of Internal Damage and Their Effect on the Behavior and Properties of Cross-Ply Composite Laminates. *International Applied Mechanics*, 38, pp.641–657. https://doi.org/10.1023/A:1020456726805
17. Mallick, P.K., 1993. *Fiber-Reinforced Composites: Materials, Manufacturing, and Design*. 2nd ed. Marcel Dekker, New York. https://doi.org/10.1201/9781420005981
18. Swain, R.E., Elmore, J.S., Lesko, J.J. and Reifsnider, K.L., The Role of Fiber, Matrix, and Interphase in the Compressive Static and Fatigue Behavior of Polymeric Matrix Composite Laminates. Book Chapter. https://doi.org/10.1520/STP24340S
19. Timmerman, J.F., Hayes, B.S. and Seferis, J.C., 2003. Cryogenic Microcracking of Carbon Fiber/Epoxy Composites: Influences of Fiber-Matrix Adhesion. *Journal of Composite Materials*, 37(21), pp.1939–1950. https://doi.org/10.1177/0021998303036281
20. Goan, J.C. and Prosen, S.P., 1969. Interfaces in Composites. *ASTM STP 452*, pp.3–26. https://doi.org/10.1002/9783527603978.mst0152
21. Drzal, L.T., Rich, M.J. and Koenig, M.E., 1983. Adhesion of Graphite Fibers to Epoxy Matrices: II. The Effect of Fiber Finish. *Journal of Adhesion*, 16(2), pp.133–152.https://doi.org/10.1080/00218468308074911
22. Schürmann, H., 2005. Konstruieren mit Faser-Kunststoff-Verbunden. Springer, Berlin/Heidelberg. https://doi.org/110.1007/b137636
23. Madhukar, M.S. and Drzal, L.T., 1991. Fiber-Matrix Adhesion and Its Effect on Composite Mechanical Properties: I. Inplane and Interlaminar Shear Behavior of Graphite/Epoxy Composites. *Journal of Composite Materials*, 25, pp.932 https://doi.org/10.1177/002199839202600701
24. Remaoun, D. and Boutaous, A., 2011. Thermomechanical stress in the evolution of shear of fiber-matrix interface composite material. *Materials Science and Applications*, 2, pp.399–403. https://doi.org/10.4236/msa.2011.25051
25. Singh, A.K. and Gupta, P.S., 2018. Evaluation of mechanical and erosive wear characteristics of TiO2 and ZnO filled bi-directional E-glass fiber based vinyl ester composites. *Silicon*, 10, pp.309–327. https://doi.org/10.1007/s12633-016-9447-3
26. Almeida, J.H.S., Amico, S.C., Botelho, E.C. and Amado, F.D.R., 2013. Hybridization Effect on the Mechanical Properties of Curaua/glass Fiber Composites. *Composites Part B: Engineering*, 55, pp.492–497. https://doi.org/10.1016/j.compositesb.2013.07.014
27. Zaer-Miri, S. and Khosravi, H., 2019. Assessment of the wear behavior and interlaminar shear properties of modified nano-TiO2/jute fiber/epoxy multiscale composites. *Journal of Industrial Textiles*, 51(7), pp.1084–1099. https://doi.org/10.1177/1528083719893718
28. Graupner, N. and Müssig, J., 2022. Interfacial and Interlaminar Shear Strength of Unidirectional Viscose Fibre-Reinforced Epoxy Composites—an Overview of the Comparability of Results Obtained by Different Test Methods. *Frontiers in Materials*, 9, pp.709845. https://doi.org/10.3389/fmats.2022.709845
29. Shoya, R., Matsuo, T., Takahashi, K., Fujimura, N. and Nakamura, T., 2021. In-situ Tensile and Fatigue Testing for Detection of Interfacial Debonding between Carbon Fibers and Epoxy Matrix by Synchrotron Radiation X-ray Nano-CT. *Journal of the Japan Society for Composite Materials*, 47(5), pp.186–193. https://doi.org/10.6089/jscm.47.186
30. Takahashi, K., Shoya, R., Matsuo, T., Sato, W., Nakamura, T., Takeuchi, A., Uesugi, M. and Uesugi, K., 2022. X-ray nanoimaging of a transversely embedded carbon fiber in epoxy matrix under static and cyclic loads. *Scientific Reports*, 12(1), pp.1–12. https://doi.org/10.1038/s41598-022-12724-1
31. Watanabe, T., Takeichi, Y., Niwa, Y., Hojo, M. and Kimura, M., 2020. Nanoscale crack initiation and propagation in carbon fiber/epoxy composites using synchrotron: 3D image data. *Data Brief*, 31, pp.105894. https://doi.org/10.1016/j.dib.2020.105894
32. Singh, D.K., Vaidya, A., Thomas, V., Theodore, M., Kore, S. and Vaidya, U., 2020. Finite Element Modeling of the Fiber-Matrix Interface in Polymer Composites.

Journal of Composites Science, 4(2), pp.58. https://doi.org/10.3390/jcs4020058
33. Sabuncuoglu, B. and Lomov, S.V., 2020. Micro-scale numerical study of fiber/matrix debonding in steel fiber composites. *Journal of Engineered Fibers and Fabrics*, 15. https://doi.org/10.1177/1558925020910726
34. Thiagarajan, P., Sain, T. and Ghosh, S., Bayesian Calibration and Uncertainty Quantification of a Rate-dependent Cohesive Zone Model for Polymer Interfaces. *Computational Engineering, Finance, and Science*, arXiv:2311.07768v1. https://doi.org/10.48550/arXiv.2311.07768
35. Ivens, J., Wevers, M., Verpoest, I. and De Meester, P., 1989. Influence of the Fibre-Matrix Interface On the Matrix Crack Development in Carbon-Epoxy Cross-Ply Laminates. In: Bunsell, A.R., Lamicq, P., Massiah, A. (eds) *Developments in the Science and Technology of Composite Materials*. Springer, Dordrecht, pp.64. https://doi.org/10.1007/978-94-009-1123-9_64
36. COMSOL Multiphysics® v. 6.3, COMSOL AB, Stockholm, Sweden. www.comsol.com
37. Matzenmiller, A., Lubliner, J. and Taylor, R.L., 1995. A constitutive model for anisotropic damage in fiber-composites. *Mechanics of Materials*, 20, pp.125–152. https://doi.org/10.1016/0167-6636(94)00053-0
38. Chihaoui, B., Serra-Parareda, F., Tarrés, Q., Espinach, F.X., Boufi, S. and Delgado-Aguilar, M., 2020. Effect of the Fiber Treatment on the Stiffness of Date Palm Fiber Reinforced PP Composites: Macro and Micromechanical Evaluation of the Young's Modulus. *Polymers*, 12(8), pp.1693. https://doi.org/10.3390/polym12081693
39. Fallahi, H., Kaynan, O. and Asadi, A., 2023. Insights into the effect of fiber–matrix interphase physiochemical-mechanical properties on delamination resistance and fracture toughness of hybrid composites. *Composites Part A: Applied Science and Manufacturing*, 166, pp.107390. https://doi.org/10.1016/j.compositesa.2022.107390
40. Goda, I., Padayodi, E. and Raoelison, R.N., 2024. Enhancing fiber/matrix interface adhesion in polymer composites: Mechanical characterization methods and progress in interface modification. *Journal of Composite Materials*, 58(29), pp.3077–3110. https://doi.org/10.1177/00219983241283958
41. Lewis, C., Yavuz, B.O., Longana, M.L., Belnoue, J.P.-H., Ramakrishnan, K.R., Ward, C. and Hamerton, I., 2024. A Review on the Modelling of Aligned Discontinuous Fibre Composites. *Journal of Composites Science*, 8(8), pp.318. https://doi.org/10.3390/jcs8080318
42. Ahmadvash Aghbash, S., Verpoest, I., Swolfs, Y. and Mehdikhani, M., 2023. Methods and models for fibre–matrix interface characterisation in fibre-reinforced polymers: a review. *International Materials Reviews*, 68(8), pp.1245–1319. https://doi.org/10.1080/09506608.2023.2265701
43. Trimiño, L.F. and Cronin, D.S., 2016. Evaluation of Numerical Methods to Model Structural Adhesive Response and Failure in Tension and Shear Loading. *Journal of Dynamic Behavior of Materials*, 2, pp.122–137. https://doi.org/10.1007/s40870-016-0045-7
44. Mubarak, A. and Joshi, S., Energy Absorption Characteristics of Interface Modified GFRP Laminates under Low Velocity Impact. *Advanced Materials Research*, 626, pp.589–593. https://doi.org/10.4028/www.scientific.net/AMR.626.589
45. Tan, W. and Martínez-Pañeda, E., 2021. Phase field predictions of microscopic fracture and R-curve behaviour of fibre-reinforced composites. *Composites Science and Technology*, 202, pp.108539. https://doi.org/10.1016/j.compscitech.2020.108539
46. Qiao, P. and Chen, Y., 2008. Cohesive fracture simulation and failure modes of FRP–concrete bonded interfaces. *Theoretical and Applied Fracture Mechanics*, 49(2), pp.213–225. https://doi.org/10.1016/j.tafmec.2007.11.005
47. Holmes, G.A., Hunston, D.L., McDonough, W.G. and Peterson, R.C., A New Methodology for Determining Interfacial Shear Strength in Single Fiber Composites. SAMPE-ACCE-DOE-SPE (Reproduction) Midwest Advanced Materials and Processing Conferences Session: Durability, pp.321–331.
48. Mantič, V., Távara, L., Blázquez, A., Graciani, E. and París, F., Application of a linear elastic-brittle interface model to the crack initiation and propagation at fibre-matrix interface under biaxial transverse loads. arXiv:1311.4596. https://doi.org/10.48550/arXiv.1311.4596
49. Hillberry, B.M. and Johnson, W.S., 1990. Matrix Fatigue Crack Development In A Nontched Continuous Fiber SCS-6/Ti-15-3 Composite. *NASA Technical Memorandum*, 102751.
50. Zhu, Y., Zhang, Y. and Xiang, L., 2025. Crack Propagation Behavior Modeling of Bonding Interface in Composite Materials Based on Cohesive Zone Method. *Buildings*, 15(10), pp.1717. https://doi.org/10.3390/buildings15101717
51. Drvoderic, M., Pletz, M. and Schuecker, C., 2022. Modeling Stiffness Degradation of Fiber-Reinforced Polymers Based on Crack Densities Observed in Off-Axis Plies. *Journal of Composites Science*, 6(1), pp.10. https://doi.org/10.3390/jcs6010010
52. Shen, B. and Paulino, G.H., 2011. Direct Extraction of Cohesive Fracture Properties from Digital Image Correlation: A Hybrid Inverse Technique. *Experimental Mechanics*, 51, pp.143–163. https://doi.org/10.1007/s11340-010-9342-6
53. Wan, L., Ismail, Y., Sheng, Y., Yang, D. and Ye, J., 2023. A review on micromechanical modelling of progressive failure in unidirectional fibre-reinforced composites. *Composites Part C: Open Access*. https://doi.org/10.1016/j.jcomc.2023.100348
54. Nagaraja, S., Elhaddad, M., Ambati, M. et al., 2019. Phase-field modeling of brittle fracture with multi-level hp-FEM and the finite cell method. *Computational Mechanics*, 63, pp.1283–1300. https://doi.org/10.1007/s00466-018-1649-7
55. Chamis, C.C., 1972. Mechanics Of Load Transfer at The Fiber/Matrix Interface. *NASA Technical Memorandum*, Washington, D.C., February.
56. Yu, Y., Zheng, X., Li, P. and Xiao, J., Progressive failure simulation of composite materials using the anisotropic phase field method. *Materials Science*. https://doi.org/10.48550/arXiv.2212.01969
57. Fan, C., Shan, Z., Zou, G. et al., 2021. Interfacial Bonding Mechanism and Mechanical Performance of Continuous Fiber Reinforced Composites in Additive Manufacturing. *Chinese Journal of Mechanical Engineering*, 34, pp.21. https://doi.org/10.1186/s10033-021-00538-7
58. Lei, Z., Li, X., Qin, F. and Qiu, W., 2014. Interfacial micromechanics in fibrous composites: design, evaluation, and models. *Scientific World Journal*, 2014, pp.282436. https://doi.org/10.1155/2014/282436
59. Motta de Castro, E., Tabei, A., Cline, D.B.H. et al., 2025. New insights in understanding the fiber-matrix interface and its reinforcement behavior using single fiber fragmentation data. *Advanced Composites and Hybrid Materials*, 8(5). https://doi.org/10.1007/s42114-024-01054-7